

# Time-periodic Metallic Metamaterials defined by Floquet Circuits

S. Moreno-Rodríguez,<sup>1</sup> A. Alex-Amor,<sup>2</sup> P. Padilla,<sup>1</sup> J.F. Valenzuela-Valdés,<sup>1</sup> and C. Molero<sup>1</sup>

<sup>1</sup>Department of Signal Theory, Telematics and Communications, Universidad de Granada (CITIC-UGR), 18071 Granada, Spain

<sup>2</sup>Department of Information Technologies, Universidad San Pablo-CEU, CEU Universities, Campus Montepríncipe, 28668 Boadilla del Monte (Madrid), Spain

(\*Electronic mail: cmoleroj@ugr.es)

In this Letter, we study the scattering and diffraction phenomena in time-modulated metamaterials of metallic nature by means of Floquet equivalent circuits. Concretely, we focus on a time-periodic screen that alternates between “metal” and “air” states. We generalize our previous approaches by introducing the concepts of “macroperiod” and “duty cycle” to the time modulation. This allows to analyze time-periodic metallic metamaterials whose modulation ratios are, in general, rational numbers. Furthermore, with the introduction of the duty cycle, perfect temporal symmetry is broken within the time modulation as the time screen could remain a different amount of time in metal and air states. Previous statements lead to an enrichment of the diffraction phenomenon and to new degrees of freedom that can be exploited in engineering to control the reflection and transmission of electromagnetic waves. Finally, we present some analytical results that are validated with a self-implemented finite-difference time-domain (FDTD) approach. Results show that the scattering level and diffraction angles can be controlled independently by means of the duty cycle and the modulation ratio, respectively. Thus, novel time-based pulsed sources and beamformers can be efficiently designed.

The resolution of electromagnetic problems based on periodic structures has classically benefited from systematic simplifications thanks to the use of Floquet’s theorem<sup>1,2</sup>. That is, the reduction of the complexity of the whole structure to a waveguide problem<sup>3</sup>. Circuit models have proven to be very efficient tools to emulate waveguide environments<sup>4-6</sup>. Simple models avoid the *dynamic* behavior of the structure, combining transmission lines and quasi-static elements<sup>7</sup>. More sophisticated proposals include the contribution of higher-order modes/harmonics<sup>8-10</sup>. This implies the validity of the models for scenarios where higher-order harmonics have a leading role<sup>11</sup>. This scenario is, for instance, quite common in time-varying systems, or in a more general context, in spacetime structures<sup>12</sup>.

Spacetime systems introduce time, generally in the form of a periodic modulation, as a new degree of freedom<sup>13-17</sup>. Though pioneering studies were theoretically reported in the middle of last century<sup>18,19</sup>, they have regained interest in the recent years, especially when non-reciprocity<sup>20,21</sup> was sought as a substitute of magnetic materials for insulators<sup>22</sup>. Some other impressive properties have since then been reported, as new temporal mechanisms for amplification<sup>23</sup>, subharmonic mixing<sup>24</sup>, giant bianisotropy<sup>25</sup>, negative refraction<sup>26</sup> or an equivalent of the Brewster angle<sup>27</sup>. Novel applications, just to name a few, are proposed in the propagation domain focused on DOA estimation<sup>28</sup>, imaging<sup>29</sup>, or digital processing<sup>30</sup>.

Transmission-line and ABCD-parameter models have already been employed in electromagnetic systems with instantaneous temporal interfaces<sup>31,32</sup>. Such are the cases reported in<sup>33,34</sup> and more recently in<sup>35</sup>. The equivalent circuit aids for a better understanding of the situations there described. However, in most cases, no periodic modulation exists and there is no excitation of higher-order harmonics. The work in<sup>36</sup> considers a system formed by a metallic screen suffering a periodic modulation. The system is fed by an external plane wave, exciting an infinite number of periodic Floquet harmonics. The paper reports the derivation of the circuit model but no many situations are evaluated. The present work is intended

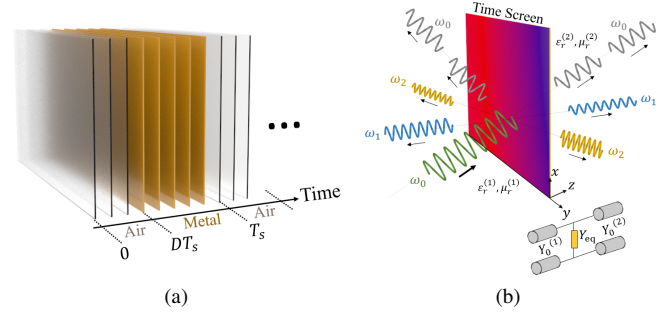


FIG. 1: (a) Time evolution of the proposed configuration. The screen periodically alternates between “air” and “metal” states. (b) Illustration of the spacetime diffraction caused by the time-periodic screen and its equivalent circuit.

to exploit the model possibilities, increasing the number of modulation ratios, introducing the concepts of *macroperiod* and *duty cycle* to the time modulation, with the objective of enriching the diffraction phenomenon. In addition, the scattering parameters are quantitatively evaluated, constituting a novelty with respect previous works in the literature.

The structure under consideration is sketched in Fig. 1. A monochromatic plane wave of frequency  $\omega_0$  illuminates a time metamaterial that periodically alternates between “air” and “metal” (perfect electric conductor, PEC) states, as represented in Fig. 1(a). The time screen is considered to be infinitesimally thin along the  $z$  axis and very large in  $x$  and  $y$  directions [see Fig. 1(b)]. The time periodicity of the varying screen is  $T_s = 2\pi/\omega_s$ , from which the whole cycle repeats. In the more general scenario, the time screen could remain in air state ( $DT_s$ ) for a different time than it remains in metal state ( $[1-D]T_s$ ). Here,  $D \in [0, 1]$  is the *duty cycle* of the time modulation. Extreme cases  $D = 0$  and  $D = 1$  would imply that the time screen remains invariant in metal and air states the whole time, respectively. The fact of varying the duty cycle  $D$  and

its implications were not discussed in our previous work<sup>36</sup>, since a fixed value of  $D = 0.5$  was implicitly assumed. As it will be detailed later, modifying the duty cycle enriches the diffraction phenomenon, since half-period temporal symmetry is broken and this leads to asymmetries in harmonic excitation. The *modulation ratio*  $F = \omega_0/\omega_s = T_s/T_0$  constitutes a second factor to be discussed. The nature of the reflected and transmitted fields across the discontinuity directly depends on this parameter, and as it will be discussed below, it may govern the power transfer between different harmonics.

Ideally, the implementation of a time-periodic thin screen that transits between "metal" and "air" states would require of a reconfigurable material whose electrical properties can be tuned in real time. Two-dimensional materials such as graphene and its oxides<sup>37</sup>, or monolayer molybdenum disulfide (MOS<sub>2</sub>)<sup>38</sup> and hexagonal boron nitride (h-BN)<sup>39</sup> are potential candidates for this purpose. For instance, it is well known that biased graphene can behave as a good electrical conductor (low surface-resistance value), being able to recreate the metal state. As the bias conditions are relaxed, the surface resistance of graphene increases, leading to absorption and transparent ("air"-like) states<sup>40,41</sup>. This properties of graphene have been exploited for the design of reconfigurable devices with advanced functionalities<sup>42</sup>.

The guidelines to derive the equivalent circuit are elaborately reported in<sup>36</sup>. The propagation of the incident and reflected waves, and the transmitted one are represented by transmission lines with  $Y_0^{(1)}$  and  $Y_0^{(2)}$  characteristic admittances, respectively. The equivalent admittance  $Y_{eq}$  accounts for the effect of the *time discontinuity*, and includes the effect of all the higher-order harmonics  $E_n$ . In general, Floquet coefficients  $E_n$  are computed as

$$E_n^{(1)} = E_n^{(2)} = \frac{1}{T_m} \int_0^{T_m} E(t) e^{-j\omega_n t} dt, \quad (1)$$

where  $\omega_n = \omega_0 + n2\pi/T_m$  is the angular frequency associated to the  $n$ -th Floquet harmonic. Moreover, the reflection ( $R$ ) and transmission ( $T$ ) coefficients, both associated to the fundamental harmonic ( $n = 0$ ), can be directly estimated from the circuit model as

$$R = \frac{Y_0^{(1)} - Y_0^{(2)} - Y_{eq}}{Y_0^{(1)} + Y_0^{(2)} + Y_{eq}}, \quad (2)$$

$$T = 1 + R. \quad (3)$$

The coupling between harmonics, described in terms of transformers with turn ratio  $N(\omega_n)$ , demands a previous knowledge of the field profile  $\mathbf{E}(t)$  at the discontinuity along a time period. Our previous work is focused on integer time-modulation ratios  $F$ , assuming  $\omega_s \leq \omega_0$  in most cases. This is a very restricted situation. The extension from integer to rational (not irrational) modulation ratios is here taken into account, modifying the way to get  $\mathbf{E}(t)$ . Now,  $\mathbf{E}(t)$  is influenced by  $D$  and  $F$ , leading to the definition of the term *macroperiod*. A macroperiod  $T_m$  is defined as the minimum time periodicity

where both the incident-wave vibration ( $\omega_0$ ) and the screen variation ( $\omega_s$ ) complete a full cycle simultaneously.

Mathematically, every *rational* modulation ratio  $F$  can be approximated by a fraction of two integers,  $F_N$  and  $F_D$ , according to  $F = F_N/F_D$ . Since  $F$  was previously defined as  $F = T_s/T_0$ , the temporal macroperiod  $T_m$  must follow the condition

$$T_m = F_N T_0 = F_D T_s. \quad (4)$$

Thus, a macroperiod is completed after  $F_N$  and  $F_D$  cycles for the incident wave ( $T_0$ ) and the time modulation ( $T_s$ ), respectively. Please note that an *irrational* modulation ratio  $F$  cannot be described in terms of a fraction of two integers, leading to an infinite set of decimals. As a consequence, the macroperiod of an irrational modulation ratio would be infinite and the formulation proposed here would not be applicable since time periodicity is lost. Thus, the field profile  $\mathbf{E}(t)$  is therefore defined along a macroperiod, ensuring a stationary situation. It can be mathematically described as

$$\mathbf{E}(t) = \sin(\omega_0 t) P(t) \hat{\mathbf{y}}, \quad t \in [0, T_m], \quad (5)$$

where  $P(t)$  is a pulse train of period  $T_s$  and duty cycle  $D$ .

Figs. 2(a)-(c) depict the evolution of  $E(t) = |\mathbf{E}(t)|$ , when the modulation ratio is fixed to  $F = 4$  ( $F = F_N/F_D = 4/1$ ), for duty cycles  $D = 0.25, 0.5, 0.75$ , respectively. In these cases, the value of the *macroperiod*  $T_m$  coincides with  $T_s$  (or  $4T_0$ ). A second case regarding  $F$  as a rational number is exhibited in Figs. 2(d)-(f), where it can be appreciated how the shape of  $E(t)$  becomes more complex. Now  $F = 1.6 = 8/5$ , increasing the macroperiod up to  $T_m = 5T_s$  or, analogously,  $T_m = 8T_0$ . In all these figures  $E(t)$  is drawn in a time interval defined by two consecutive macroperiods, in order to appreciate the existing periodicity. As will be explained below, the variation of  $D$  has direct implications on the amplitude provided by each Floquet harmonic.

A correct definition of  $E(t)$  is crucial to guarantee accurate predictions by the circuit model. A first test of the validity of the circuit approach is shown in Fig. 3. It illustrates the normalized spectral response of the transmitted field in the cases reported in Fig. 2, with an inset showing the field profile  $E(t)$ . A TM-polarized plane wave impinging normally has been assumed for the computation. As expected, the spectrum is split in discrete harmonics, whose amplitudes vary for each case. Together with the results provided by the equivalent circuit, numerical results extracted by self-implemented finite-different time-domain (FDTD) are included. FDTD methods<sup>43,44</sup> have proven to be interesting numerical alternatives to validate analytical results due to the absence of specific commercial electromagnetic solvers oriented to deal with spacetime metamaterials. It is also worthy to emphasise that due to assumption of normal incidence, all the harmonics are propagative (there is no harmonics with evanescent nature) and moreover, they leave the air-metal interface at the incidence direction ( $\theta_n = 0^\circ$ ). This result comes from Eq.[28]

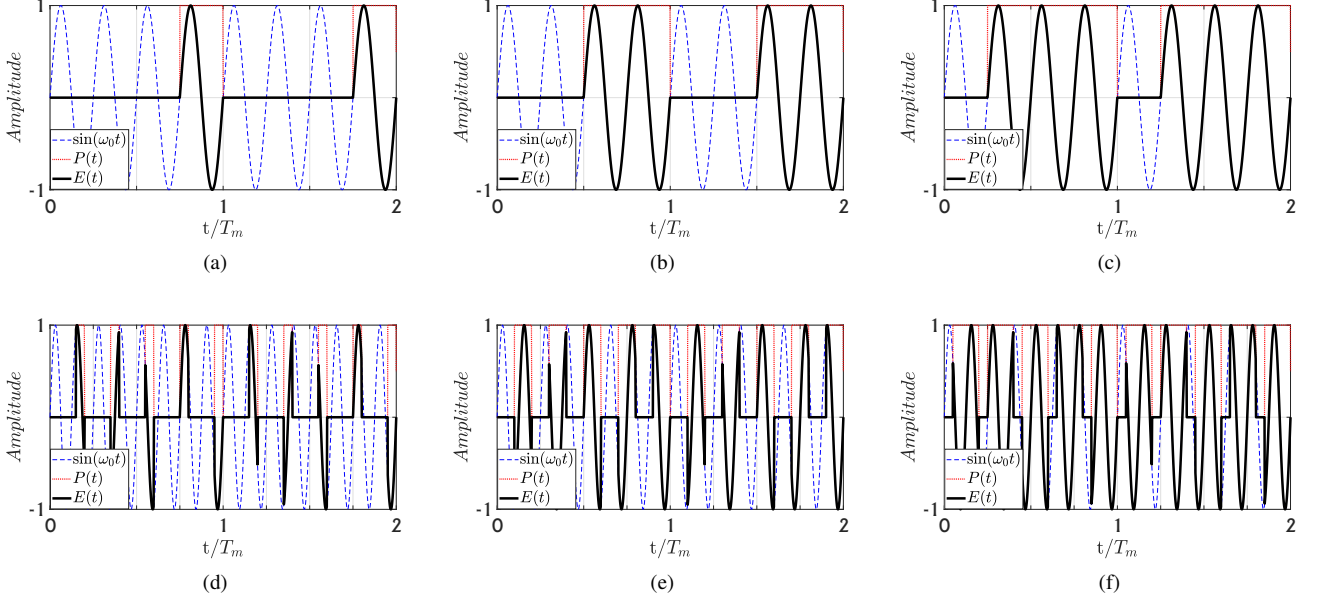


FIG. 2: Two macroperiods of  $E(t)$  when: (a)  $F = 4$ ,  $D = 0.25$ , (b)  $F = 4$ ,  $D = 0.5$ , (c)  $F = 4$ ,  $D = 0.75$ , (d)  $F = 1.6$ ,  $D = 0.25$ , (e)  $F = 1.6$ ,  $D = 0.5$ , (f)  $F = 1.6$ ,  $D = 0.75$ .

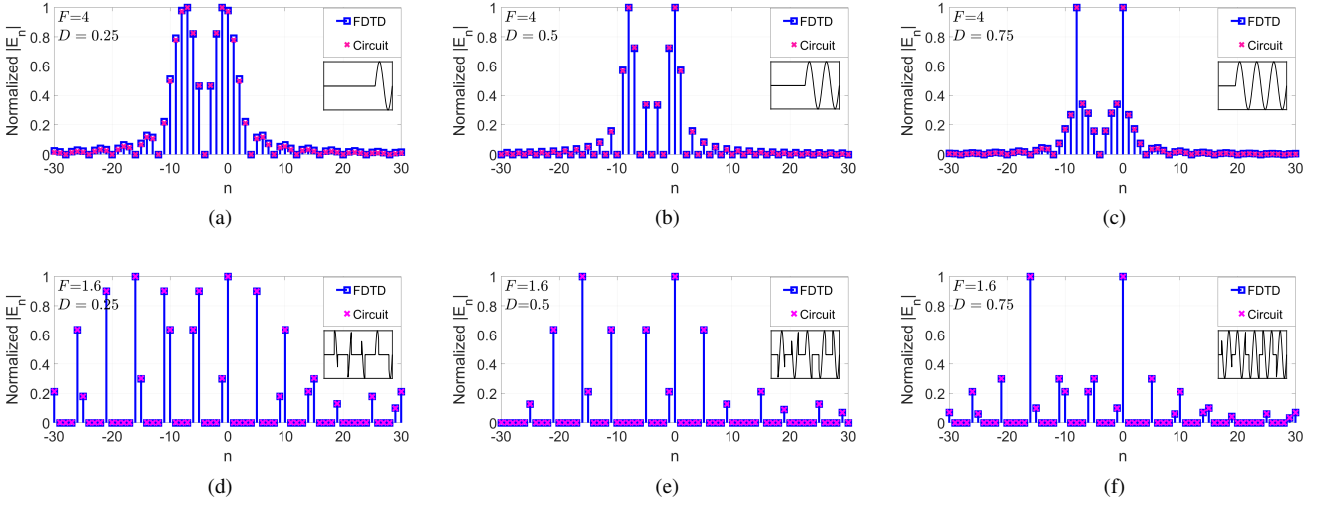


FIG. 3: Normalized amplitude of the Floquet coefficients in the cases: (a)  $F = 4$ ,  $D = 0.25$ , (b)  $F = 4$ ,  $D = 0.5$ , (c)  $F = 4$ ,  $D = 0.75$ , (d)  $F = 1.6$ ,  $D = 0.25$ , (e)  $F = 1.6$ ,  $D = 0.5$ , (f)  $F = 1.6$ ,  $D = 0.75$ . Normal incidence is assumed.

in<sup>36</sup>

$$\theta_n^{(i)} = \arctan \left( \frac{k_t}{\sqrt{\epsilon_r^{(i)} \mu_r^{(i)} \left[ \frac{\omega_0 + 2\pi n/T_m}{c} \right]^2 - k_t^2}} \right) \quad (6)$$

when imposing  $k_t = 0$  with  $k_t$  being the transverse wavevector of the incident wave, and  $i = 1, 2$  being the index indicating the leftmost/ rightmost medium respectively.

As visualized in Figs. 3(a)-(c) for  $F = 4$ , the value of  $D$  modifies the amplitude of the harmonics. For instance, when

the wave encounters free-space in a longer time interval than metal at the interface,  $D = 0.75$ , the biggest amplitude values are carried by the fundamental harmonic ( $n = 0$ ) and that with order  $n = -8$  [see Fig. 3(c)]. When this interval decreases to  $D = 0.25$ , the amplitude of these predominant harmonics reduces with respect the rest of diffracted harmonics [see Fig. 3(a)]. This tendency seems to be progressive if we check Figs. 3(a)-(c) from left to right. If the modulation ratio is varied down to  $F = 1.6$ , as illustrated in the spectra shown in Figs. 3(d)-(f), it can be noticed that the modal distance between harmonics have changed. This fact can be appreciated

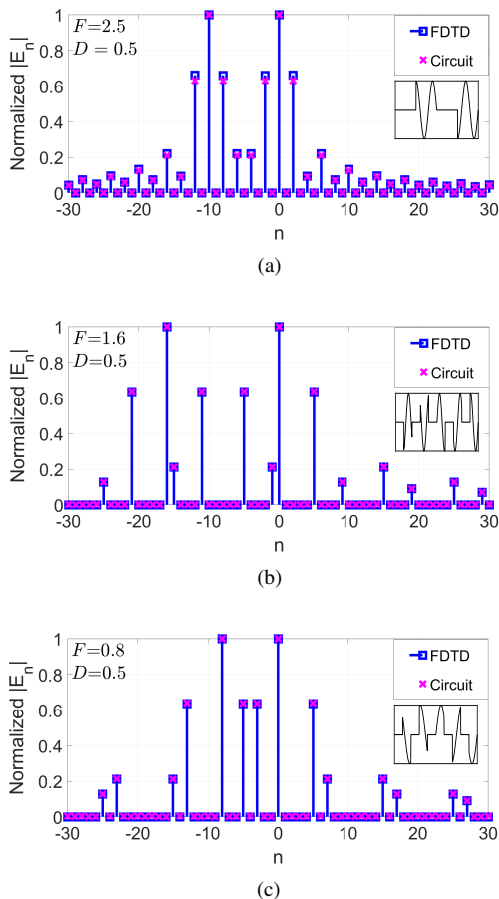


FIG. 4: Normalized amplitude of the Floquet coefficients in the cases: (a)  $F = 2.5$ ,  $D = 0.5$ , (b)  $F = 1.6$ ,  $D = 0.5$ , (c)  $F = 0.8$ ,  $D = 0.5$ . Oblique incidence is assumed:  $\theta_{\text{inc}} = 30^\circ$ .

since those carrying more energy are now the fundamental one ( $n = 0$ ) and the one with order  $n = -16$ . In general, increasing the duty cycle  $D$  provokes that the time screen remains in "air" state a greater amount of time. Thus, the field profile  $\mathbf{E}(t)$  progressively turns into the original incident plane wave as  $D$  approaches the unit. Therefore, the spectrum of the system resembles the spectrum of a conventional sine function, predominated by two delta functions at frequencies  $\pm\omega_0$ , with the rest of harmonics being significantly attenuated. This phenomenon is observed in Figs. 3(a)-(c) and Figs. 3(d)-(f) as  $D$  is increased. Note that breaking the perfect temporal symmetry of the modulation ( $D \neq 0.5$ ) causes that harmonics of even and odd nature excite indistinctly. The situation was different in our previous work<sup>36</sup>, where the duty cycle was fixed to  $D = 0.5$ . In that case, perfect temporal symmetry provoked that higher-order even harmonics became null, fact that can be also appreciated in Figs. 3(b) and (e). Therefore, the introduction of the duty cycle to the time modulation enriches the diffraction spectrum, which is of potential interest for the development of time-based beamformers.

To understand the effect of the reconfigurability in this time-periodic metamaterial, Fig. 4 shows configurations with different modulation ratios  $F$  while keeping the same duty cy-

TABLE I: Diffraction angle  $\theta_n$  of the main Floquet harmonics while applying different modulation ratios. Oblique incidence is considered:  $\theta_{\text{inc}} = 30^\circ$ . The duty cycle of the time-periodic screen is  $D = 0.5$ .

	Diffacted Angle	Circuit	FDTD
$F = 2.5$	$\theta_{-2}(\circ)$	56.44	56.49
	$\theta_0(\circ)$	30	29.97
	$\theta_2(\circ)$	20	20.05
$F = 1.6$	$\theta_0(\circ)$	30	30.05
	$\theta_5(\circ)$	17.92	17.92
$F = 0.8$	$\theta_0(\circ)$	30	30.01
	$\theta_5(\circ)$	12.89	12.91

cle fixed to  $D = 0.5$ . This situation consisting is well captured by the circuit model, after a previous definition of  $E(t)$ . The temporal evolution of  $E(t)$  along a macroperiod is included as an inset of the figures. Now, TE oblique incidence is assumed under an angle of incidence  $\theta_{\text{inc}} = 30^\circ$ . The transverse wavevector is no longer null ( $k_t \neq 0$ ), opening the possibility to excite evanescent harmonics according to (6). Fig. 4(a) depicts a first case governed by  $F = 2.5$ . For this configuration, some evanescent harmonics have non-zero amplitude values, as those with orders  $n = -6, -4$ . The rest of harmonics with non-zero amplitude are propagative. As  $F$  changes, the amplitude distribution get modified. In case illustrated in Fig. 4(b) the modulation ratio is  $F = 1.6$ , and now the evanescent harmonics with significant amplitude are those with orders  $n = -11, -5$ . For  $F = 0.8$ , reported in Fig. 4(c), they become the ones with orders  $n = -5, -3$ .

The harmonics with propagative nature appearing in Fig. 4 now scatters in different directions. The diffraction angles of each propagating harmonic have been calculated using (6). They have been compared with the angles obtained by FDTD in TABLE I. As observed, there is a good agreement between both analytical (Floquet circuit) and numerical results. Naturally, one point to note is the difference in simulation times for each solution. The analytical Floquet solution reduces notably the computational complexity compared to the FDTD. Concretely, the circuit model requires a simulation time of the order of seconds, while the FDTD takes minutes to simulate the scenario. This becomes more evident as the macroperiod of the time-modulated metamaterial is larger.

Subsequently, Fig. 5 illustrates the electric field distribution in the transmission region ( $z > 0$ ) for the cases reported in Fig. 4. Fig. 5(a) considers  $F = 2.5$  and  $D = 0.5$ . The time screen is located at  $z/\lambda_0 = 0$ . As  $F$  substantially decreases, it can be noticed that the diffraction angle of higher-order harmonics separate from that of the fundamental harmonic ( $\theta_0 = 30^\circ$ ), approaching the normal direction ( $\theta_n \approx 0^\circ$ ). This is well predicted by (6). It is worth remarking that the harmonic orders appearing in TABLE I are those whose amplitude contribution is significant in the field representation of Fig. 5. The rest of harmonics taking place in the whole field expansion have not been included for some reasons: their amplitude is not significant and are not appreciated in the FDTD;

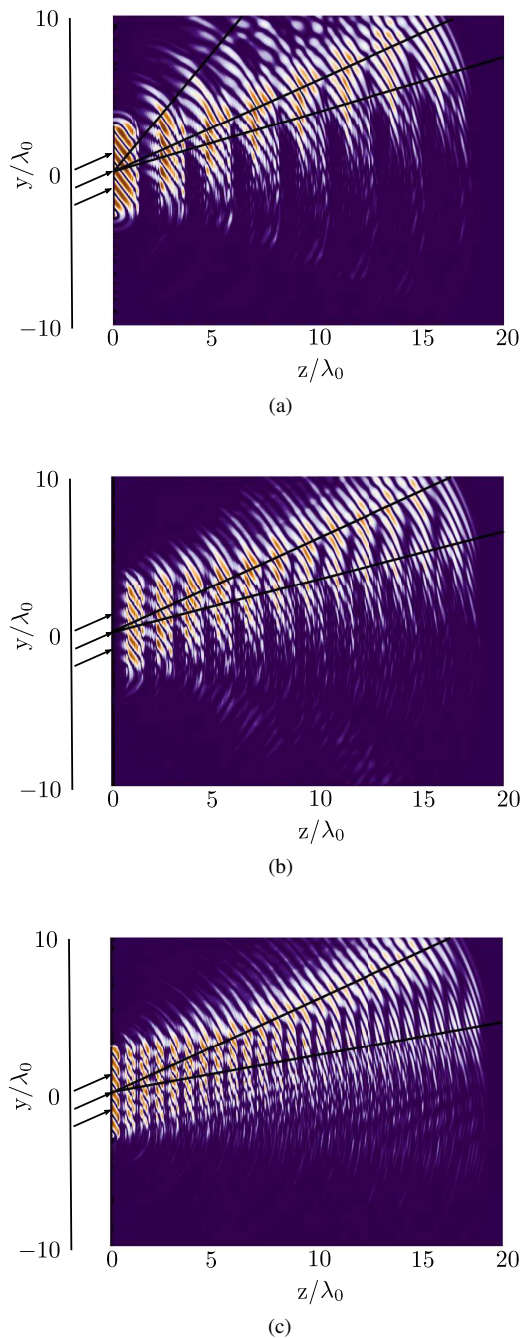


FIG. 5: Electric field distribution obtained with the FDTD method in the cases: (a)  $F = 2.5$ ,  $D = 0.5$ , (b)  $F = 1.6$ ,  $D = 0.5$ , (c)  $F = 0.8$ ,  $D = 0.5$ .

they have an evanescent nature; they propagate backwards ( $\beta_n^{(2)} < 0$ ).

Finally, Fig. 6 shows the transmission coefficient  $T$ , related to the fundamental harmonic ( $n = 0$ ), for several values of the modulation ratio  $F$  and duty cycle  $D$ . Normal incidence is now considered, though oblique incidence can straightforwardly be computed. A comparison is illustrated between the results extracted from the Floquet circuit and the FDTD

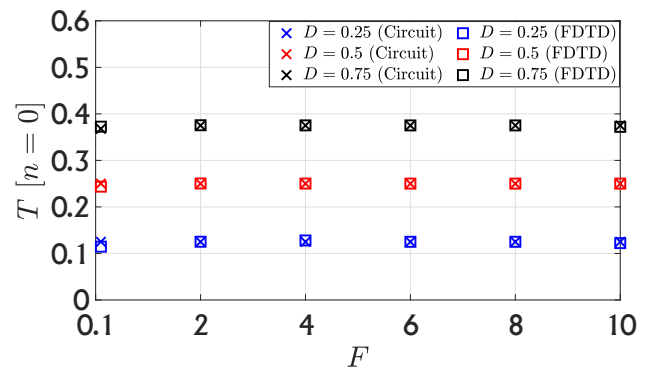


FIG. 6: Transmission coefficient  $T$  as a function of the modulation ratio  $F$  for different duty cycles  $D$ .

method, showing a good agreement. It can be appreciated that, for a fixed duty cycle, the transmission coefficient remains constant regardless of the value of the modulation ratio. Conversely, the transmission coefficient increases as the duty cycle does. This is due to the fact that the time-periodic screen remains a greater amount of time in the "air" state than in the "metal" state, allowing the incident waves to pass through it more easily in average.

To conclude, in this Letter, we have studied the diffraction of electromagnetic fields produced by an incident plane wave with TE/TM polarization impinging on a time-periodic metallic screen. The proposed time-modulated metamaterial periodically alternates between "air" and "metal" states, leading to the excitation of diffraction orders that can be exploited to manipulate the propagation of electromagnetic waves. We have carried out the analysis by means of two tools: an analytical Floquet circuit and a numerical FDTD method. By introducing the concepts of "macroperiod" ( $T_m$ ) and "duty cycle" ( $D$ ) to the time modulation, we have extended the beamforming capabilities of the temporal structure shown in our previous works. The reconfigurability of higher-order modes has been discussed as a function of changes in the modulation ratio  $F$  and the duty cycle  $D$ . These results open up the possibility to simulate time-varying structures in a much more faster and efficient way than other full-wave electromagnetic tools, with the aim of designing novel time-based microwave and photonic devices.

## ACKNOWLEDGMENTS

This work was supported in part by the Spanish Government under Projects PID2020-112545RB-C54, TED2021-129938B-I00 and TED2021-131699B-I00; in part by "Junta de Andalucía" under Project A-TIC-608-UGR20, Project P18.RT.4830, and Project PYC20-RE-012-UGR; in part by a Leonardo Grant of the BBVA foundation. The authors acknowledge the support of the BBVA foundation for the funds associated to a project belonging to the program Leonardo Grants 2021 for researchers and cultural creators from the BBVA foundation. The BBVA Foundation accepts no respon-

sibility for the opinions, statements and contents included in the project and/or the results thereof, which are entirely the responsibility of the authors.

## DATA AVAILABILITY

The data that support the findings of this study (analytical Floquet circuit and numerical FDTD codes) are available from the corresponding author upon reasonable request.

## REFERENCES

- <sup>1</sup>C. Elachi, “Waves in active and passive periodic structures: A review,” *Proceedings of the IEEE* **64**, 1666–1698 (1976).
- <sup>2</sup>A. Alex-Amor, A. Palomares-Caballero, and C. Molero, “3-D metamaterials: Trends on applied designs, computational methods and fabrication techniques,” *Electronics* **11**, 410 (2022).
- <sup>3</sup>J. E. Varela and J. Esteban, “Characterization of waveguides with a combination of conductor and periodic boundary contours: Application to the analysis of bi-periodic structures,” *IEEE Transactions on Microwave Theory and Techniques* **60**, 419–430 (2012).
- <sup>4</sup>N. Marcuvitz, *Waveguide Handbook* (Institution of Electrical Engineers, GBR, 1986).
- <sup>5</sup>F. Costa, A. Monorchio, and G. Manara, “Efficient analysis of frequency-selective surfaces by a simple equivalent-circuit model,” *IEEE Antennas and Propagation Magazine* **54**, 35–48 (2012).
- <sup>6</sup>F. Mesa, R. Rodríguez-Berral, and F. Medina, “Unlocking complexity using the ECA: The equivalent circuit model as an efficient and physically insightful tool for microwave engineering,” *IEEE Microwave Magazine* **19**, 44–65 (2018).
- <sup>7</sup>O. Luukkonen, C. R. Simovski, G. Granet, G. Goussetis, D. V. Lioubtchenko, A. V. Raisanen, and S. A. Tretyakov, “Simple and accurate analytical model of planar grids and high-impedance surfaces comprising metal strips or patches,” *IEEE Transactions on Antennas and Propagation* **56**, 1624–1632 (2008).
- <sup>8</sup>R. Rodríguez-Berral, F. Mesa, and F. Medina, “Analytical multimodal network approach for 2-D arrays of planar patches/apertures embedded in a layered medium,” *IEEE Transactions on Antennas and Propagation* **63**, 1969–1984 (2015).
- <sup>9</sup>A. Alex-Amor, F. Mesa, A. Palomares-Caballero, C. Molero, and P. Padilla, “Exploring the potential of the multi-modal equivalent circuit approach for stacks of 2-d aperture arrays,” *IEEE Transactions on Antennas and Propagation* **69**, 6453–6467 (2021).
- <sup>10</sup>C. Molero, A. Alex-Amor, F. Mesa, A. Palomares-Caballero, and P. Padilla, “Cross-polarization control in FSSs by means of an equivalent circuit approach,” *IEEE Access* **9**, 99513 (2021).
- <sup>11</sup>C. Molero, R. Rodríguez-Berral, F. Mesa, F. Medina, M. Memarian, and T. Itoh, “Planar resonant blazed gratings from a circuit model standpoint,” *IEEE Transactions on Antennas and Propagation* **68**, 2765–2778 (2020).
- <sup>12</sup>S. Taravati and G. V. Eleftheriades, “Generalized space-time-periodic diffraction gratings: Theory and applications,” *Phys. Rev. Applied* **12**, 024026 (2019).
- <sup>13</sup>V. Pacheco-Peña, D. M. Solís, and N. Engheta, “Time-varying electromagnetic media: opinion,” *Opt. Mater. Express* **12**, 3829–3836 (2022).
- <sup>14</sup>C. Caloz and Z.-L. Deck-Léger, “Spacetime metamaterials—part i: General concepts,” *IEEE Transactions on Antennas and Propagation* **68**, 1569–1582 (2020).
- <sup>15</sup>C. Caloz and Z.-L. Deck-Léger, “Spacetime metamaterials—part ii: Theory and applications,” *IEEE Transactions on Antennas and Propagation* **68**, 1583–1598 (2020).
- <sup>16</sup>K. J. Deshmukh and G. W. Milton, “An energy conserving mechanism for temporal metasurfaces,” *Applied Physics Letters* **121**, 041702 (2022).
- <sup>17</sup>E. Galiffi, R. Tirole, S. Yin, H. Li, S. Vezzoli, P. A. Huidobro, M. G. Silveirinha, R. Sapienza, A. Alù, and J. B. Pendry, “Photonics of time-varying media,” *Advanced Photonics* **4**, 014002 (2022).
- <sup>18</sup>F. Morgenthaler, “Velocity modulation of electromagnetic waves,” *IRE Transactions on Microwave Theory and Techniques* **6**, 167–172 (1958).
- <sup>19</sup>T. Tamir, H. Wang, and A. Oliner, “Wave propagation in sinusoidally stratified dielectric media,” *IEEE Transactions on Microwave Theory and Techniques* **12**, 323–335 (1964).
- <sup>20</sup>J. Zang, D. Correias-Serrano, J. Do, X. Liu, A. Alvarez-Melcon, and J. Gomez-Diaz, “Nonreciprocal wavefront engineering with time-modulated gradient metasurfaces,” *Phys. Rev. Applied* **11**, 054054 (2019).
- <sup>21</sup>D. L. Sounas and A. Alu, “Non-reciprocal photonics based on time modulation,” *Nature Photonics* **11**, 774–783 (2017).
- <sup>22</sup>S. Taravati, N. Chamanara, and C. Caloz, “Nonreciprocal electromagnetic scattering from a periodically space-time modulated slab and application to a quasisonic isolator,” *Phys. Rev. B* **96**, 165144 (2017).
- <sup>23</sup>J. B. Pendry, E. Galiffi, and P. A. Huidobro, “Gain in time-dependent media—a new mechanism,” *J. Opt. Soc. Am. B* **38**, 3360–3366 (2021).
- <sup>24</sup>Z. Wu, C. Scarborough, and A. Grbic, “Space-time-modulated metasurfaces with spatial discretization: Free-space  $N$ -path systems,” *Phys. Rev. Applied* **14**, 064060 (2020).
- <sup>25</sup>P. Huidobro, M. Silveirinha, E. Galiffi, and J. Pendry, “Homogenization theory of space-time metamaterials,” *Phys. Rev. Applied* **16**, 014044 (2021).
- <sup>26</sup>V. Bruno *et al.*, “Negative refraction in time-varying strongly coupled plasmonic-antenna-epsilon-near-zero systems,” *Phys. Rev. Lett.* **124**, 043902 (2020).
- <sup>27</sup>V. Pacheco-Peña and N. Engheta, “Temporal equivalent of the brewster angle,” *Phys. Rev. B* **104**, 214308 (2021).
- <sup>28</sup>X. Fang, M. Li, J. Han, D. Ramaccia, A. Toscano, F. Bilotti, and D. Ding, “Low-complexity doa estimation method based on space-time modulated metasurfaces,” in *2022 IEEE International Symposium on Antennas and Propagation and USNC-URSI Radio Science Meeting (AP-S/URSI)* (2022) pp. 1282–1283.
- <sup>29</sup>B. H. Kolner, “Space-time imaging, magnification, and time reversal of matter waves,” *Applied Physics Letters* **117**, 124001 (2020).
- <sup>30</sup>L. Li, H. Zhao, C. Lui, and T. Jun Cui, “Intelligent metasurfaces: control, communication and computing,” *eLight* **2** (2022).
- <sup>31</sup>Y. Xiao, D. N. Maywar, and G. P. Agrawal, “Reflection and transmission of electromagnetic waves at a temporal boundary,” *Opt. Lett.* **39**, 574–577 (2014).
- <sup>32</sup>S. Y. Elnaggar and G. N. Milford, “Modeling space-time periodic structures with arbitrary unit cells using time periodic circuit theory,” *IEEE Transactions on Antennas and Propagation* **68**, 6636–6645 (2020).
- <sup>33</sup>D. Ramaccia, A. Toscano, and F. Bilotti, “Light propagation through metamaterial temporal slabs: reflection, refraction, and special cases,” *Opt. Lett.* **45**, 5836–5839 (2020).
- <sup>34</sup>D. Ramaccia, A. Alù, A. Toscano, and F. Bilotti, “Temporal multilayer structures for designing higher-order transfer functions using time-varying metamaterials,” *Applied Physics Letters* **118**, 101901 (2021).
- <sup>35</sup>L. Stefanini, S. Yin, D. Ramaccia, A. Alù, A. Toscano, and F. Bilotti, “Temporal interfaces by instantaneously varying boundary conditions,” *Phys. Rev. B* **106**, 094312 (2022).
- <sup>36</sup>A. Alex-Amor, S. Moreno-Rodríguez, P. Padilla, J. F. Valenzuela-Valdés, and C. Molero, “Time-varying metallic interfaces,” (2022), <https://doi.org/10.48550/arXiv.2206.09684>.
- <sup>37</sup>W. Yu, L. Sisi, Y. Haiyan, and L. Jie, “Progress in the functional modification of graphene/graphene oxide: a review,” *RSC Adv.* **10**, 15328–15345 (2020).
- <sup>38</sup>X. Li and H. Zhu, “Two-dimensional MoS<sub>2</sub>: Properties, preparation, and applications,” *Journal of Materiomics* **1**, 33–44 (2015).
- <sup>39</sup>A. Laturia, M. Van de Put, and W. Vandenberghe, “Dielectric properties of hexagonal boron nitride and transition metal dichalcogenides: from monolayer to bulk,” *npj 2D Mater Appl* **2** (2018).
- <sup>40</sup>M. J. Allen, V. C. Tung, and R. B. Kaner, “Honeycomb carbon: A review of graphene,” *Chemical Reviews* **110**, 132–145 (2010).
- <sup>41</sup>S.-E. Zhu, S. Yuan, and G. C. A. M. Janssen, “Optical transmittance of multilayer graphene,” *Europhysics Letters* **108**, 17007 (2014).
- <sup>42</sup>C. Molero, A. Palomares-Caballero, A. Alex-Amor, I. Parellada-Serrano, F. Gamiz, P. Padilla, and J. F. Valenzuela-Valdés, “Metamaterial-based reconfigurable intelligent surface: 3D meta-atoms controlled by graphene structures,” *IEEE Communications Magazine* **59**, 42–48 (2021).

<sup>43</sup>S. A. Stewart, T. J. Smy, and S. Gupta, "Finite-difference time-domain modeling of space-time-modulated metasurfaces," *IEEE Transactions on Antennas and Propagation* **66**, 281–292 (2018).

<sup>44</sup>Y. Vahabzadeh, N. Chamanara, and C. Caloz, "Generalized sheet transition condition ftd simulation of metasurface," *IEEE Transactions on Antennas and Propagation* **66**, 271–280 (2018).